IOP Publishing Journal of Physics: Condensed Matter
J. Phys.: Condens. Matter **34** (2022) 185701 (11pp) https://doi.org/10.1088/1361-648X/ac303b

Modeling oxidised polypyrrole in the condensed phase with a novel force field

Yoseph Abere, Greg Helmick and Estela Blaisten-Barojas[*]

Center for Simulation and Modeling and Department of Computational and Data Sciences, George Mason University, 4400 University Drive, Fairfax, VA 22030, United States of America

E-mail: blaisten@gmu.edu

Received 10 August 2021, revised 10 October 2021
Accepted for publication 15 October 2021
Published 3 March 2022

Abstract
A novel model potential is developed for simulating oxidised oligopyrroles in condensed phases. The force field is a coarse grained model that represents the pyrrole monomers as planar rigid bodies with fixed charge and dipole moment and the chlorine dopants as point atomic charges. The analytic function contains 17 adjustable parameters that are initially fitted on a database of small structures calculated within all-electron density functional theory. A subsequent potential function refinement is pursued with a battery of condensed phase isothermal–isobaric Metropolis Monte Carlo in-silico simulations at ambient conditions with the goal of implementing a hybrid parametrization protocol enabling agreement with experimentally known thermodynamic properties of oxidised polypyrrole. The condensed system is composed of oligomers containing 12 monomers with a 1:3 dopant-to-monomer concentration. The final set of force field optimised parameters yields an equilibrium density of the condensed system at ambient conditions in excellent agreement with oxidised polypyrrole samples synthesised in wet-laboratories.

Keywords: PPy, oxidised oligopyrrole, polypyrrole force field, Metropolis Monte Carlo simulation, conducting polymers

(Some figures may appear in colour only in the online journal)

1. Introduction

Polypyrrole (PPy) is a conjugated polymer that exists naturally and is easily manufactured. The polymer was discovered in 1963 [1]. In 1974 it became very popular with the advent of the first electronic device [2] showing the unusual conducting properties of this class of conjugated polymers. Currently, PPy is catalogued as a prototypical conducting polymer or organic metal with unique mechanical, optical, electrical and chemical properties. PPy is a polycationic conductor when oxidised that loses its electrical conduction upon reduction. In fact, pristine neutral PPy is a semiconductor with a band gap of 3.0 eV. The oxidised phase is attained upon doping such that p-type conduction (holes) occurs in the polymeric matrix. It is the easiness with which PPy can flip from the oxidised phase to the reduced phase that makes this polymer so attractive for device fabrication. The fast charging/discharging property has been exploited in batteries [3, 4] and sensors [5]. In chemical catalysts and new clean energy efficient technologies, PPy is used in low temperature fuel cells to mediate and increase the catalyst dispersion on the graphite support layers [6]. More traditional uses include PPy sensitised cathode electrocatalysts that enhance reduction activity of metallic electrocatalysts [7]. The synthesis of carbon nanotubes on PPy substrates is enhanced due to the ability of the polymer to absorb microwave radiation and elevate the reaction temperature to several hundred °C [8]. Meanwhile, PPy applications in medicine have increased significantly in the last years. For example, the use of PPy for artificial muscles has notorious advantages over motor actuators [9–13]. The ability of oxidised PPy by anionic dopants for nerve growth and survival has shown critical for ensuring optimal delivery of neurotrophins in inner-ear therapies [14]. The potential of PPy as a material for tissue engineering is high [15].

---

[*] Author to whom any correspondence should be addressed.

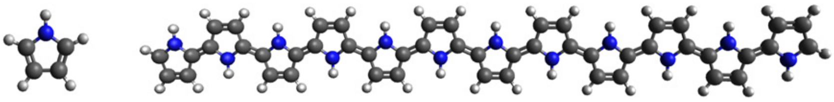

Figure 1. The pyrrole molecule (left) and the 12-monomer oligopyrrole in the quinoid (oxidised) phase, 12-Py (right).

PPy is obtained from polymerization of the heterocyclic pyrrole (Py) molecule C_4H_4NH (figure 1). The Py backbone has alternating single and double C–C bonds that create a conjugated π bond system across the oligomer length. Synthesised PPy is obtained in the laboratory in the oxidised phase [10]. A posterior redox reaction yields the neutral, reduced phase. In the oxidised phase the polymerization rate is hindered because of charge recombination leading to polymer matrices composed of short oligomers in the range of 6–18 monomers only [16]. The conjugated backbone of oxidised (charged) PPy is of quinoid type with double C–C bonds joining the monomers, as shown in figure 1 for an oligomer with 12 monomers. Meanwhile, in the case of reduced (neutral) PPy the conjugation type switches to benzenoid with C–C single bonds between the monomers. Polymer matrices of these oligopyrroles do not crystallise. However, in the solid phase there are macromolecular assemblies such as columnar formations, chain stacking and lamellar domains [17]. These structural formations depend on the type of dopants used in the PPy synthesis. A variety of dopants are used experimentally such as small inorganic anions (chlorine, iodine, etc), benzene sulfonate and p-toluene sulfonate among other aromatic anions [10], and biologically active anions [14].

Several theoretical studies based on density functional theory (DFT) have investigated the structure, energetics and electronic properties of oligopyrrole in the gas phase [18, 19]. Oxidised oligopyrrole most stable backbone has monomers in the anti-gauge conformation [18]. However, it is still computationally challenging to scale up the quantum mechanical calculations to systems in condensed phases that are not crystalline. Both Metropolis Monte Carlo (MC) and molecular dynamics (MD) methods enable simulation of dense phases based on model classical potentials describing the interactions of the constituent molecules. Simulation methodologies rely heavily on the force field (FF) employed. López Cascales *et al* [20, 21] studied the condensed phases of 10-Py oxidised oligomers at polymer-solvent interfaces with the GROMOS(1987) FF of GROMACS 3.3.3 [22] parametrised for condensed phase properties of alkanes. Dai and Blaisten-Barojas [19] developed a coarse grained FF for reduced Py and studied the thermodynamics and structure of 12-Py oligopyrroles in the solid phase using the Adaptive Tempering Monte Carlo [23]. A combined synthesis/simulation work [16] synthesised oxidised Py samples with chlorine dopants showing polymer stacking at sample densities between 1300–1450 kg m^{-3}. The corresponding MD simulations with OPLS-AA FF were able to achieve solid systems of oligomers with 6 and 12 monomers that yielded lower densities than their synthetic counterparts for dopant concentrations of 25%.

Here we develop a coarse grained FF well adapted for simulations of oxidised PPy in the condensed phases. We consider condensed systems composed of oligopyrroles with 12 monomers, size that fall within the range of 8 to 16 obtained in the syntheses of condensed PPy [24], doped with atomic chlorine. A correct classical representation of a system of charged components, both the oligopyrroles and the atomic dopants, is not trivial. During the oxidation process there is important charge transfer from the oligopyrrole chains to the electronegative dopants. Based on our previous DFT study of oxidised oligopyrroles [18] and the previously developed FF for reduced PPy [19], oxidised oligomers with 12 pyrrole monomers (therein termed 12-Py) have acquired a $+4e$ charge by transferring electrons to four chlorine $-1e$ anions. These anionic dopants remain trapped between the cationic 12-Py for maintaining charge neutrality at a dopant/monomer concentration of 33%. High oxidation levels enabled an 80% improved polymer conductivity [16]. The new FF is generalisable for oxidised PPy systems that give rise to bipolarons [25] in which oligomer regions of consecutive monomers sustain a charge of $+2e$ due to charge transfer to electronegative dopants. In oxidised 12-Py there are two of such regions [18].

The paper is organised as follows. Section 2 provides a description of the computational methods employed and the modeling adopted for the condensed phase of the oxidised PPy system. The FF developed is presented in section 3. Each Py monomer is modeled as a planar rigid molecule with charge and permanent dipole anchored at the centre of mass and each chlorine dopant is modeled as a point negative charge. This section provides the analytic description of the intra-oligomer interactions between monomers and the corresponding description of the inter-interactions, including monomer-dopant and monomer–monomer terms between different oligomers, and dopant–dopant interactions. Section 4 presents the workflow used in the FF parameter optimisation which includes the use of a database of geometries and electronic energies of small oligopyrrole structures doped with chlorine atoms as target points for the fitting process. This section includes a description of why and when MC simulations were needed for refining the FF parameters determination. The section contains results on the thermodynamics and structure of the oxidised PPy system in the condensed phase at ambient conditions. This work is concluded in section 5. The appendix contains the doped 12-Py structures included in the database of structures.

2. Methods and models

Development of the proposed coarse grained model entailed four components for determining the parameters involved: (i) a quantum mechanics DFT approach for both, determining the charge transfer occurring from polymer to chlorine dopants in oxydised 12-Py chains as depicted in figure 2, (ii) a battery

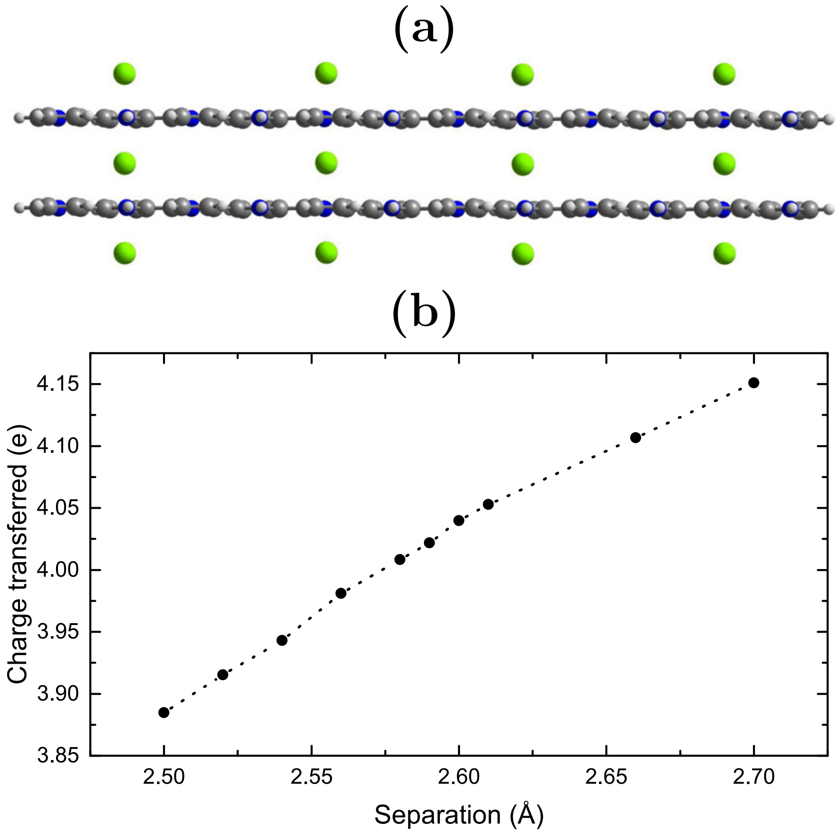

Figure 2. (a) Structure of oxidised 12-Py oligomers with chlorine dopants (depicted green) used for determining the charge transfer; (b) charge transferred from each 12-Py oligomer to the dopants as function of the monomer-dopant separation distance.

of DFT calculations for establishing the energetics of twelve small structures of the oxidised system as function of dopant-polymer distance and orientation that yielded 122 target binding energy points, (iii) a non-linear least squares fit of the 17 parameters in the analytical function of the FF provided in section 3 that used the 122 DFT-calculated target energy values, and (iv) testing of the obtained parameters by performing a MC simulation on a system containing 64 12-Py chains and 256 chlorine dopants at 300 K and 1 atm. For the charge transfer process the structure shown in figure 2(a) was used. The group of structures employed for energetics are depicted in figure A1 of the appendix, while an initial configuration of the polymer matrix is illustrated in figure 3. The process was iterative as is described below.

All DFT calculations were performed at the B3PW91 hybrid functional level with Grimme's empirical dispersion correction [26] and the 6-311g(d) basis set [27]. The calculated atomic charges were obtained from the electrostatic potential surface following the Merz–Singh–Kollman scheme [28, 29]. We used this DFT methodology as implemented in the Gaussian 09 package [30], with self consistent electronic energies obtained within 10^{-8} precision.

The atomic charges entering in the proposed FF of section 3 resulted from the DFT-calculated polymer-dopant charge transfer. Figure 2(a) depicts the structure used with that purpose. Meanwhile figure 2(b) illustrates that a loss of $+4e$ per 12-Py oligomer occurred at about 2.6 Å resulting in +4 cation oligopyrroles. The electric dipole moment μ of the 12-Py^{+4} monomers was also determined at this DFT level yielding a value of 1.4 D (Debye units). Atomic charges and monomer dipole were not considered to be FF variable parameters.

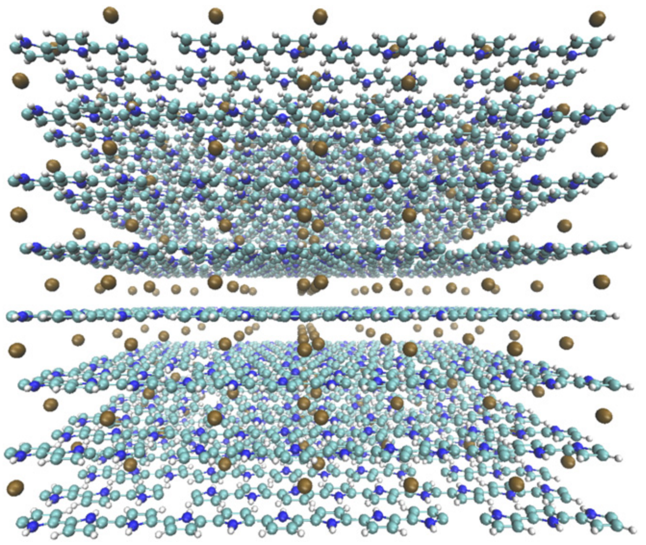

Figure 3. Initial simulation configuration of 64 12-Py oligomers and 256 dopants positioned in the sites of a 1 × 4 × 4 orthorhombic lattice with periodic boundary conditions. Dopants are ochre, oligomer carbon atoms are cyan, nitrogens are blue and hydrogens are white.

The DFT binding energy of structures in figure A1 yielded 122 target points on which the 17 parameters of the proposed

FF were fitted. Among these structures, the top six in figure A1 were used for determining the FF intra-oligomer terms. Three structures with two or three monomers were considered to be +1 cations while the three 12-Py structures were considered as +4 cations. The electronic state of all these structures was a singlet. In figure A1, the six structures used for determining the inter oligomer–oligomer, oligomer–dopant, and dopant–dopant terms groups of oligomers with 4 chlorine dopants per 12-Py were neutral. Each of these structures generated several geometries by displacing angles or distance marked by arrows in figure A1. The number of points associated to such displacements for each structure is reported in parenthesis in figure A1.

The DFT-calculated binding energies were the target points on which the parameters of the FF described in section 3 were fitted. The fitting process was achieved using the Levenberg–Marquardt algorithm [31, 32] for obtaining the minimum of the least non-linear squares error between the DFT binding energy target points and the model potential values at the same geometry of the considered structures of figure A1.

After an initial set of FF parameters were obtained, multiple MC simulations were performed, both for very small structures with a few 12-Py oligomers and systems containing 64 12-Py oligomers in condensed phases. The MC method is a Markov chain MC that generates a concatenated sequence of configurations based upon sampling from the Boltzmann distribution [33]. The MC simulations were implemented in the isothermal–isobaric ensemble (NPT) with an in-house, custom implementation [34, 35] of the sampling acceptance rule $\min\left\{1, \exp\left(-\left[\Delta U + P(V_n - V_o) - (N+1)\ln(V_n/V_o)\right]/k_\mathrm{B}T\right)\right\}$ for moving from old-to-new configurations [36]. Here: $\Delta U = U(\mathbf{s_n}^N, V_n) - U(\mathbf{s_o}^N, V_o)$ with $\mathbf{s_n}^N$, $\mathbf{s_o}^N$ being the scaled N particle coordinates in the new (n) and old (o) configurations with system volumes V_n, V_o, respectively, P, T are the system fixed pressure and temperature, and k_B is the Boltzmann constant.

MC runs were needed for validating the performance of the FF parameters at different temperatures and densities. Thus, a feedback between new DFT calculations, new fittings, and new MC simulations was established as described in section 4.

For the MC simulations, a fairly cubic computational box was built placing 64 12-Py oligomers and 256 dopants at the sites of a 1 × 4 × 4 orthorhombic lattice with constants $a = 4.475$ nm, $b = 1.106$ nm, $c = 1.006$ nm. This system is small, with 1024 particles but large enough for the desired testing of the FF. Figure 3 illustrates the initial computational box employed in the simulations. Periodic boundary conditions were used with a cutoff radius R_cut of 19 Å, characteristic of simulations at 300 K and 1 atm. A MC *iteration* was defined by the attempted move of all the 1024 particles in the box. Simulations were run on the order of 2×10^6 MC iterations.

3. The force field description and its parametrisation

The approach adopted in the FF for reduced oligopyrrole [19] is now altered such that each monomer in 12-Py is represented as a planar rigid body having a $q = 1/3e$ fractional charge located at its centre of mass with an anchored permanent dipole moment $\mu = 1.4$ D pointing towards the nitrogen atom. Dopants are atomic chlorine atoms with a charge $Q = -1e$. The analytical form of our previous FF for reduced oligopyrroles [19] is supplemented with new added terms that account for the Coulomb interactions as well as for interactions monomer–dopant and dopant–dopant. The new FF has 17 adjustable parameters that are fitted to the DFT-calculated target points composing the structure database illustrated in figure A1. Two additional parameters are embedded in the Coulomb interactions, which are modeled within the Wolf *et al* [37] approach that damps the long range contribution via a κ parameter and shifts the potential to nil beyond a cutoff R_cut. In a nutshell, the total potential energy of the system is split into intra-oligomer interactions:

$$U_\mathrm{Total} = U_\mathrm{intra} + U_\mathrm{inter}. \tag{1}$$

The intra-oligomer potential is given by seven terms:

$$\begin{aligned} U_\mathrm{intra} = {} & U_\mathrm{bond} + U_\mathrm{bend} + U_\mathrm{torsion} + U_\mathrm{lib} + U_\mathrm{elec} \\ & + U_\mathrm{dipole-dipole} + U_\mathrm{anti-coil}. \end{aligned} \tag{2}$$

The terms composing the U_intra are described in section 3.1 and U_inter interactions are presented in section 3.2.

3.1. Intra-potential interactions

The bonding term, U_bond, is a Morse potential function [38] that links the centres of mass of two contiguous monomers within each oligomer:

$$U_\mathrm{bond} = D_e \sum_{i=1}^{n-1} \left[\left(1 - \mathrm{e}^{-\alpha\left(\frac{r_{i,i+1}}{r_0} - 1\right)} \right)^2 - 1 \right], \tag{3}$$

where $r_{i,i+1}$ are the function variables identifying distances between two contiguous monomer centres of mass in one 12-Py with $n = 12$. Constants $D_e = 2.6921$ eV, $r_0 = 3.78569$ Å, $\alpha = 3.32146$ are the fitted parameters. The bending term U_bend models the concerted planar motion between any three-contiguous monomers:

$$U_\mathrm{bend} = k_\theta \sum_{i=2}^{n-1} (\cos(\theta_i) - \cos(\theta_0))^2, \tag{4}$$

where the variables are θ_i angles between the $i-1, i, i+1$ monomers. The fitted parameters are $k_\theta = 26.12$ eV, and $\theta_0 = 141.576°$. The torsion term U_torsion involves motion of the the dihedral angle formed by the four contiguous atoms N–C=C–C between two contiguous monomers:

$$\begin{aligned} U_\mathrm{torsion} = \sum_{i=1}^{n-1} & \left[k_1 \left(1 - \cos(\gamma_{i,i+1} - \gamma_0)\right) \right. \\ & \left. + k_2 \left(1 - \cos 2(\gamma_{i,i+1} - \gamma_0)\right) \right], \end{aligned} \tag{5}$$

where the variables are $\gamma_{i,i+1}$, dihedral angles between consecutive monomers. The fitted parameters are $k_1 = 0.0548$ eV,

$k_2 = 0.3795$ eV, and $\gamma_0 = 180°$. The libration term U_{lib} relates to a monomer's hindered rotation around a fixed axis normal to each monomer's plane:

$$U_{\mathrm{lib}} = k_{\mathrm{lib}} \sum_{i=1}^{n} \left[\left(\cos\left(\frac{\vec{r}_{i,i+1}}{r_{i+1}} \cdot \hat{e}_i \right) + \cos(\theta_0/2) \right)^2 + \left(\cos\left(\frac{\vec{r}_{i,i-1}}{r_{i-1}} \cdot \hat{e}_i \right) + \cos(\theta_0/2) \right)^2 \right] \tag{6}$$

,where the variables are angles defined by the scalar product between vectors $\vec{r}_{i,i+1}$, $\vec{r}_{i,i-1}$ with $\widehat{e}_i$, unit vector in the plane of the ith monomer pointing from its centre of mass towards the instantaneous position of the nitrogen atom. The fitting parameter is $k_{\mathrm{lib}} = 21.35$ eV and θ_0 is the bending angle of equation (4). The U_{elec} is the Coulomb interaction between non-contiguous q-charged monomers:

$$U_{\mathrm{elec}} = \frac{q^2}{4\pi\epsilon_0} \sum_{i=1}^{n-2} \sum_{j=i+2}^{n} \left(\frac{\mathrm{erfc}(\kappa r_{ij})}{r_{ij}} - U_{\mathrm{cut}} \right), \tag{7}$$

where r_{ij} are the variables, $q = \frac{1}{3}e$ is the monomer charge located at its centre of mass, ϵ_0 is the vacuum permittivity, erfc is the complementary error function, $U_{\mathrm{cut}} = \mathrm{erfc}(\kappa R_{\mathrm{cut}})/R_{\mathrm{cut}}$, $\kappa = 0.1134$ Å^{-1} and $R_{\mathrm{cut}} = 19$ Å were the adopted parameters. The dipole–dipole term $U_{\mathrm{dipole-dipole}}$ models the interactions between the permanent dipoles of any oligomer pair:

$$U_{\mathrm{dipole-dipole}} = \frac{1}{4\pi\epsilon_0} \sum_{i=1}^{n-1} \sum_{j=i+1}^{n} \frac{1}{r_{ij}^3} \left[\vec{\mu}_i \cdot \vec{\mu}_j - 3 \frac{(\vec{\mu}_i \cdot \vec{r}_{ij})(\vec{\mu}_j \cdot \vec{r}_{ij})}{r_{ij}^2} \right], \tag{8}$$

where r_{ij} are the variables, $\mu_{\mathrm{i}} = 1.4126$ D is the magnitude of each monomer permanent dipole moment along the direction of the corresponding unit vector $\widehat{e}_i$ of equation (6). The last term $U_{\mathrm{anti-coil}}$ is a 9-6 Mie potential function [38] that prevents the oligomer backbone from coiling:

$$U_{\mathrm{anti-coil}} = 2\epsilon_{\mathrm{intra}} \sum_{i=1}^{n-2} \sum_{j=i+2}^{n} \left[\left(\frac{\sigma_{\mathrm{intra}}}{r_{ij}} \right)^9 - \frac{3}{2} \left(\frac{\sigma_{\mathrm{intra}}}{r_{ij}} \right)^6 \right], \tag{9}$$

where the variables are r_{ij}, distances between non-contiguous monomer centres of mass. The fitted parameters are $\epsilon_{\mathrm{intra}} = 0.075\,899$ eV, $\sigma_{\mathrm{intra}} = 8.957\,44$ Å.

3.2. Inter-potential interactions

The inter component term U_{inter} comprises interactions between monomers in different 12-Py oligomers $U_{\mathrm{Py-Py}}$, interactions between monomers and dopants $U_{\mathrm{Py-dopant}}$, and dopant–dopant interactions $U_{\mathrm{dopant-dopant}}$:

$$U_{\mathrm{inter}} = U_{\mathrm{Py-Py}} + U_{\mathrm{Py-dopant}} + U_{\mathrm{dopant-dopant}}. \tag{10}$$

There are N_{Py} oligomers in the system with monomers separated by distances R_{ij} between their centres of mass. The monomer–monomer interaction term between different oligomers has three components:

$$U_{\mathrm{Py-Py}} = U_{\mathrm{elec}} + U_{\mathrm{excluded}} + U_{\mathrm{dipole-dipole}}. \tag{11}$$

The U_{elec} represents the Coulomb interaction between monomers in different oligomers, The U_{excluded} term handles the excluded volume between monomers in different oligomers preventing monomers from adjacent chains from unphysical proximity:

$$U_{\mathrm{elec}} + U_{\mathrm{excluded}} = \sum_{i=1}^{N_{\mathrm{Py}}-1} \sum_{j=i+1}^{N_{\mathrm{Py}}} \left[\frac{q^2}{4\pi\epsilon_0} \left[\frac{\mathrm{erfc}(\kappa R_{ij})}{R_{ij}} - U_{\mathrm{cut}} \right] + 2\epsilon_{\mathrm{Py-Py}} \left[\left(\frac{\sigma_{\mathrm{Py-Py}}}{R_{ij}} \right)^9 - \frac{3}{2} \left(\frac{\sigma_{\mathrm{Py-Py}}}{R_{ij}} \right)^6 \right] \right] \tag{12}$$

,where R_{ij} are the variables that stand for distances between any two monomers in different oligomers. The fitted parameters are $\epsilon_{\mathrm{Py-Py}} = 0.136$ eV and $\sigma_{\mathrm{Py-Py}} = 5.5$ Å. The $U_{\mathrm{dipole-dipole}}$ term in equation (11) describing the interaction between dipole moments of monomers in different chains has the same analytical expression as equation (8), with summations covering up to N_{Py} monomers and N_{dopant} dopants. Figure 4(a) illustrates the radial dependence of the full monomer–monomer interaction, equation (11), indicating a repulsive barrier between 8–12 Å that favours oligomer pairs of different 12-Py oligomers to be fairly well localized unless energy is provided to overcome such barrier. The $U_{\mathrm{Py-dopant}}$ term comprises sums of two pairwise interactions, Coulomb and dispersion, between the N_{Py} monomers centre mass and the N_{dopant} dopants:

$$U_{\mathrm{Py-dopant}} = \sum_{i=1}^{N_{\mathrm{Py}}} \sum_{j=1}^{N_{\mathrm{dopant}}} \left[\frac{qQ}{4\pi\epsilon_0} \left(\frac{\mathrm{erfc}(\kappa R_{ij})}{\mathrm{R}_{ij}} - U_{\mathrm{cut}} \right) + \left(A \left(\frac{\sigma_{\mathrm{Py-dopant}}}{R_{ij}} \right)^9 - B \left(\frac{\sigma_{\mathrm{Py-dopant}}}{R_{ij}} \right)^6 \right) \right] \tag{13}$$

,where the variables R_{ij} are distances between dopants and monomers. The fitted parameters are $A = 0.036\,319$ eV, $B = 0.043\,7573$ eV and $\sigma_{\mathrm{Py-dopant}} = 3.6145$ Å. For visualization purposes, equation (13) is depicted in figure 4(b) as a function of distance. These interactions are very strong, and contribute the most to the full binding of the condensed system. The $U_{\mathrm{dopant-dopant}}$ interaction has a single term and is fully repulsive:

$$U_{\mathrm{dopant-dopant}} = \sum_{i=1}^{N_{\mathrm{dopant}}-1} \sum_{j=i+1}^{N_{\mathrm{dopant}}} \left[\epsilon_{\mathrm{dopant}} \left(\frac{\sigma_{\mathrm{dopant}}}{R_{ij}} \right)^9 + \frac{Q^2}{4\pi\epsilon_0} \left(\frac{\mathrm{erfc}(\kappa R_{ij})}{R_{ij}} - U_{\mathrm{cut}} \right) \right], \tag{14}$$

where the variables R_{ij} are distances between dopants. The fitted parameters are $\epsilon_{\mathrm{dopant}} = 2.9672$ eV and $\sigma_{\mathrm{dopant}} = 4.9089$ Å.

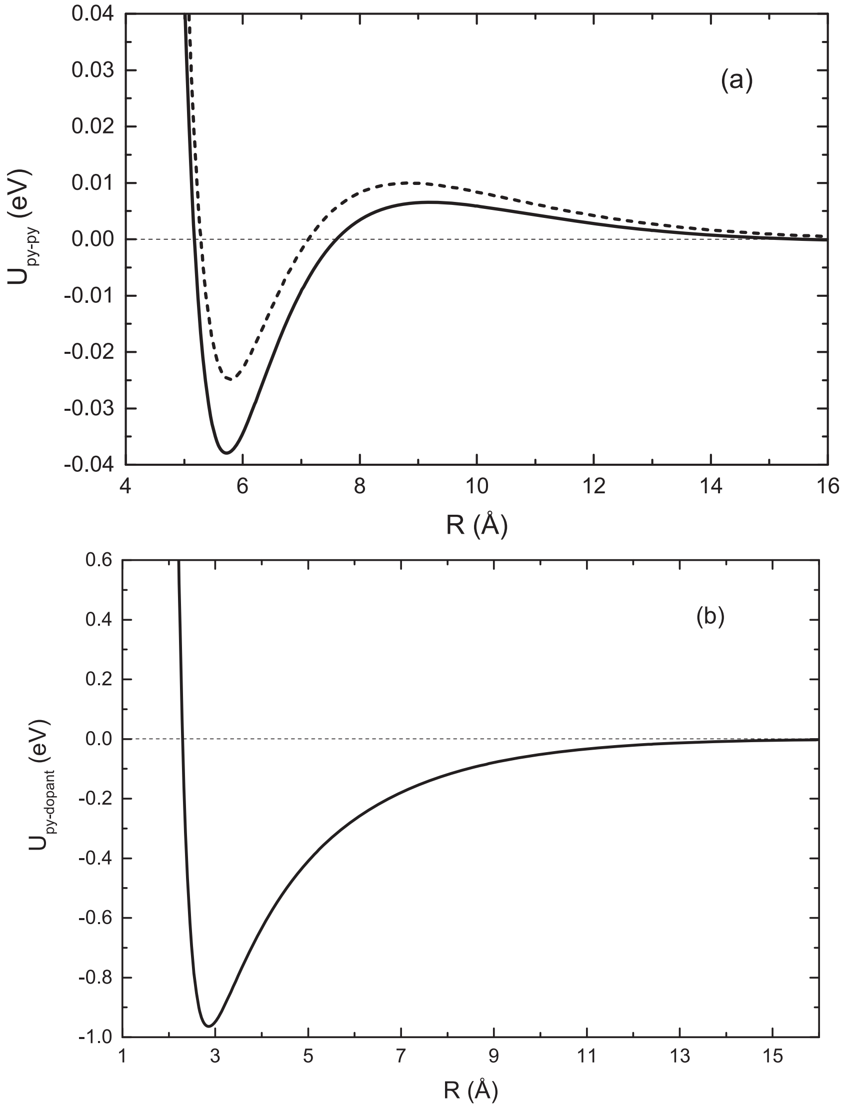

Figure 4. Interaction energies monomer-monomer in different 12-Py and monomer–dopant as a function of distance: (a) $U_{\mathrm{Py-Py}}$ of equation (11), (b) $U_{\mathrm{Py-dopant}}$ of equation (13). The solid and dotted lines in (a) depict the maximum and minimum contribution to equation (11) of $U_{\mathrm{dipole-dipole}}$ (equation (8)); the maximum occurs if the two monomers have dipole moments pointing in the same direction and the minimum is a negative value occurring when the two dipoles point in opposite directions.

4. Workflow for the force field parametrisation and evaluation

The strategy for refining the FF parameters entailed an iterative alternation between DFT calculations and MC simulations. The parameter κ entering in the Coulomb terms of equations (7) and (12)–(14) controls the damping of the charge–charge interaction with distance. Given the possibility of condensed systems simulations of small size systems and others of much larger sizes, three κ values were considered, 0.05, 0.06, 0.085 Å^{-1}. In all three cases the parameter R_{cut} in the Coulomb terms was $R_{\mathrm{cut}} = 19$ Å. In addition, Wolf's approach [37] contains a self term which is a constant once κ, the charges, and their number are given. The total potential energy calculated from the FF was referred to that electrostatic self-energy value. Parameters reported in section 3 correspond to $\kappa = 0.06$ Å^{-1}, which yielded the lowest root mean square error (RMSE) of the three κ cases. For each κ value the full process described in this section was undertaken.

The FF parametrisation and its evaluation involved two distinct stages. The first stage was dedicated to optimising the 11 intra-potential parameters of U_{intra}: D_e, r_0, α, k_θ, θ_0, k_1, k_2, γ_0, k_{lib}, $\epsilon_{\mathrm{intra}}$, and σ_{intra}. This stage involved DFT calculations only and entailed determining sequentially the bonding parameters followed by the bending, torsion and planar libration parameters fitted on 65 target structures. With that set of parameters determined, then the anti-coiling parameters were obtained keeping the previous set fixed and fitting 41 target values from the database (24 points of dimer and torsion structures were excluded). The process was iterated several times until the RMSE reached a low value of 0.49 eV particle^{-1}. A schematic visualization of this workflow is depicted in figure 5 (top panel).

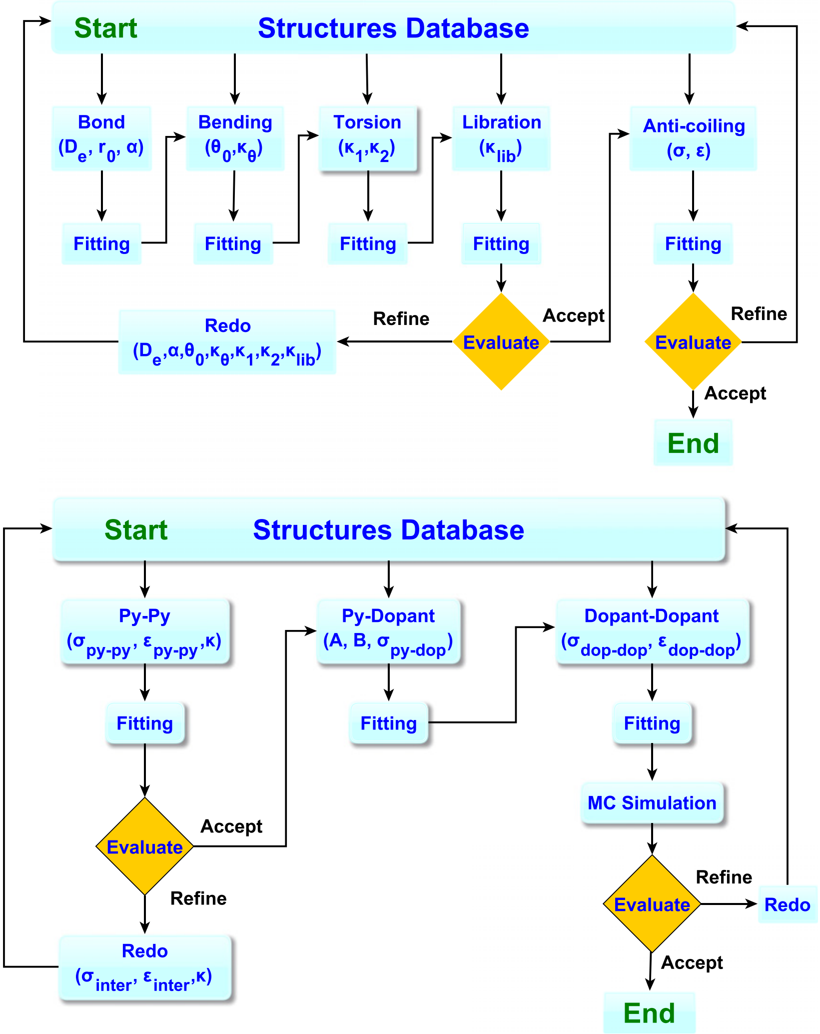

Figure 5. Workflow for determining the parameters entering in U_{intra}, equations (3)–(9) (top) and U_{inter}, equations (11), (13) and (14) (bottom).

The second stage consisted in holding the intra-potential parameters fixed whilst fitting the 8 adjustable parameters entering in the inter-potential U_{inter}: $\epsilon_{\text{Py}-\text{Py}}$, $\sigma_{\text{Py}-\text{Py}}$, A, B, $\epsilon_{\text{inter}-ee}$, $\sigma_{\text{inter}-ee}$, ϵ_{dopant}, and σ_{dopant}. This stage required both DFT calculations and MC simulations. The structure database, figure A1, contained 57 structures resulting from DFT calculations of the electronic energy as function of distances. Initially, parameters entering in $U_{\text{Py}-\text{Py}}$, $U_{\text{Py}-\text{dopant}}$, and $U_{\text{dopant}-\text{dopant}}$ (equations (12)–(14)) were independently fitted against the 57 target structures associated to the inter-terms as shown in figure 5 (bottom). The process was iterated several times until the RMSE displayed a decreasing trend. Next an MC simulation was done at temperature $T = 300$ K and 1 atm, which yielded an equilibrated system with a too low density when compared with experimental published results [16, 39–41]. Next, using the existing parameters, additional MC simulations were done changing the $\sigma_{\text{Py}-\text{Py}}$ value and keeping all the other parameters fixed until the system density stabilised around 1350 kg m^{-3}. A revision of the other inter-parameters fitting against the 57 database target points was processed, first keeping the new $\sigma_{\text{Py}-\text{Py}}$ fixed and refitting $\sigma_{\text{Py}-\text{Py}}$. The RMSE was further decreased.

This revision led to supplementary longer MC simulations of 1.5×10^6 MC iterations at 300 K and 1 atm that yielded equilibrated system densities above 1350 kg m^{-3} when keeping all parameters fixed and changing $\sigma_{\text{Py}-\text{Py}}$. Our final adoption settled for $\sigma_{\text{Py}-\text{Py}} = 5.5$ Å that gave an acceptable average density of 1410 ± 2 kg m^{-3} and a slightly lower enthalpy, as shown in figure 6. With these parameter values the final RMSE of the full fit was 0.148 eV particle^{-1}.

The system density was a specific target along the FF parameter fitting process, however, experimental values are in the range of 1200 to 1500 kg cm^{-3} depending upon the dopant size [16]. It is then interesting to also inspect how other properties behave for different densities within this range. Enthalpy, density, cohesive energy (E_{coh}), and the Hildebrand solubility parameter (δ_{h}) were calculated along the long MC trajectories providing evidence of the small fluctuations of the thermodynamic and energetic properties of the system as shown in table 1. Also evidenced from table 1 is that densities consistent with experiments have under our modeling a slight energetics

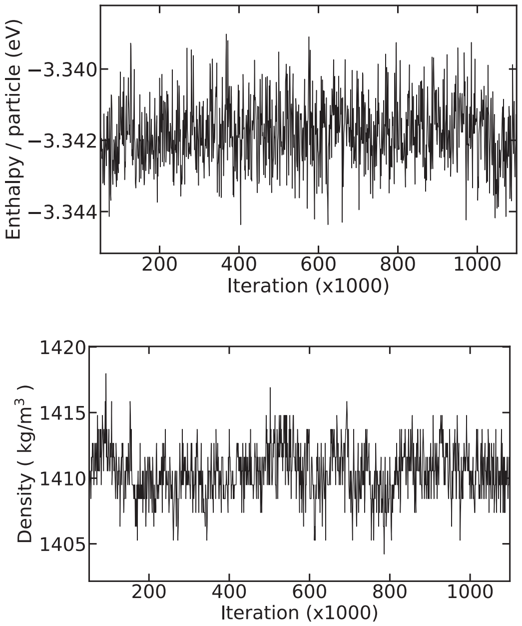

Figure 6. Enthalpy per particle and density of the system containing 64 12-Py oligomers and 256 dopants along the MC trajectory equilibrated at 300 K and 1 atm. Averages of these properties are -3.342 ± 0.001 eV and 1410 ± 2 kg m^{-3}, respectively.

Table 1. Averages of properties for the system with 64 12-Py and 256 dopants at 300 K and 1 atm for various values of $\sigma_{\mathrm{Py-Py}}$ in equation (12). U_{intra} and U_{inter} are the potential energies from equations (2) and (11), respectively. E_{coh} is the system cohesive energy, δ is the Hildebrand solubility parameter.

Properties	$\sigma_{\mathrm{Py-Py}} = 5.2$ Å	$\sigma_{\mathrm{Py-Py}} = 5.5$ Å
Enthalpy/particle (eV)	-3.210 ± 0.005	-3.342 ± 0.001
Density (kg m^{-3})	1465 ± 2	1410 ± 2
Molar volume (nm^3 mol^{-1})	0.524 ± 0.001	0.544 ± 0.001
U_{intra}/particle (eV)	-1.706 ± 0.001	-1.722 ± 0.001
U_{inter}/particle (eV)	-1.543 ± 0.006	-1.679 ± 0.001
E_{coh} (MJ mol^{-1})	152.4 ± 0.6	165.87 ± 0.07
δ_{h} (MPa$^{1/2}$)	21.71 ± 0.05	22.230 ± 0.005

cost as density increases for the small system simulated. Thus, we additionally performed simulations with lager systems with volumes increased by a factor 8 and 27 from the one considered here. In both cases the density decreased slightly and the enthalpy/particle had a gain when using the final parameters in the FF. Both, cohesive energy and Hildebrand parameter, are within values obtained for other conjugated polymers [42, 43].

Structural properties associated to the oligomers themselves were also calculated, displaying insignificant differences for the cases reported in table 1. The vector order parameter $S = \frac{1}{2}\langle 3\cos^2\beta - 1\rangle$ is a measure of the ordering/stacking of oligomers in the full system [19] with value of 1 indicating a strong spatial oligomer alignment and stacking. In this expression the brackets denote the NPT average and β is the angle between the end-to-end vector joining monomer 1 with monomer 12 in each 12-Py and the system direction vector obtained by averaging the 64 end-to-end vectors at each MC iteration. At 300 K and 1 atm, $S = 0.99$ for the set of possible parameters shown in table 1. This property evidences the agreement with experimental observations of π–π chain stacking in bulk oxidised PPy samples [9, 16, 17] and indicates that the preferential oligomer organisation in the condensed phase is not strongly dependent on the excluded volume parameter $\sigma_{\mathrm{Py-Py}}$ within the range of values investigated here. Meanwhile, from the simulation perspective, it is clear that the system underwent structural changes since the orthorhombic arrangement of the initial configuration (figure 3) was lost, whilst the molecular stacking persisted in a disordered manner, as shown in figure 7 and consistent with the obtained volume decrease of about 12.5 nm^3 due to molecular movement. On the average, the oligomers radius of gyration, end-to-end distance, and orientation order parameter Z [19] of the 12-Py oligomers in the equilibrated condensed system were 1.16 ± 0.01 nm, 3.92 ± 0.02 nm, 0.741 ± 0.002, respectively.

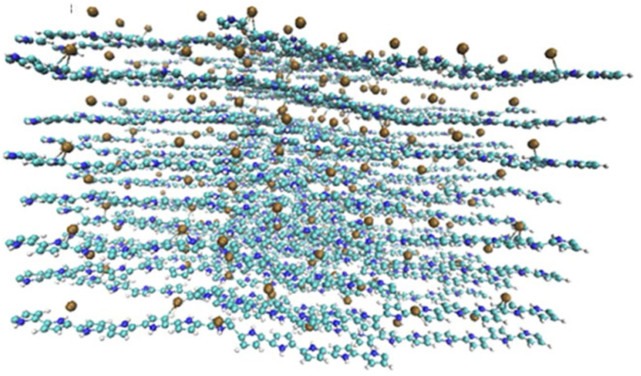

Figure 7. The final configuration of the system containing 64 12-Py and 256 dopants equilibrated at 300 K and 1 atm. Ochre is for Cl dopants, cyan for *C* atoms, blue for *N* atoms and white for *H* atoms.

5. Discussion and conclusion

The majority of previous macromolecular FF developments emphasised on improving the agreement between quantum and molecular mechanics data for monomer and very short oligomer chemistry and the parametrisation was assumed to be transferable for describing polymers with higher molecular weight in the condensed phases. More so, the interaction between the polymer chains is most frequently based on van der Waals interactions that are parametrised over pairs of different atoms from molecular databases. Non-bonded Coulomb interactions between atomic charges are also current practice, although the atomic charges are most generally calculated for monomers or small fraction of atoms in larger macromolecules. The success of such approach is undoubtedly more limited the larger the simulated system. For that reason the simulation of polymer systems in condensed phases continues to be a challenge. Accuracy control is further exacerbated by the standard use of Ewald sums schemes for the inclusion of the long range electrostatic corrections that preclude specific shapes for the simulation box containing the condensed system under study. The latter, consequently, limits the predictive scope of simulations for properties of polymeric systems in

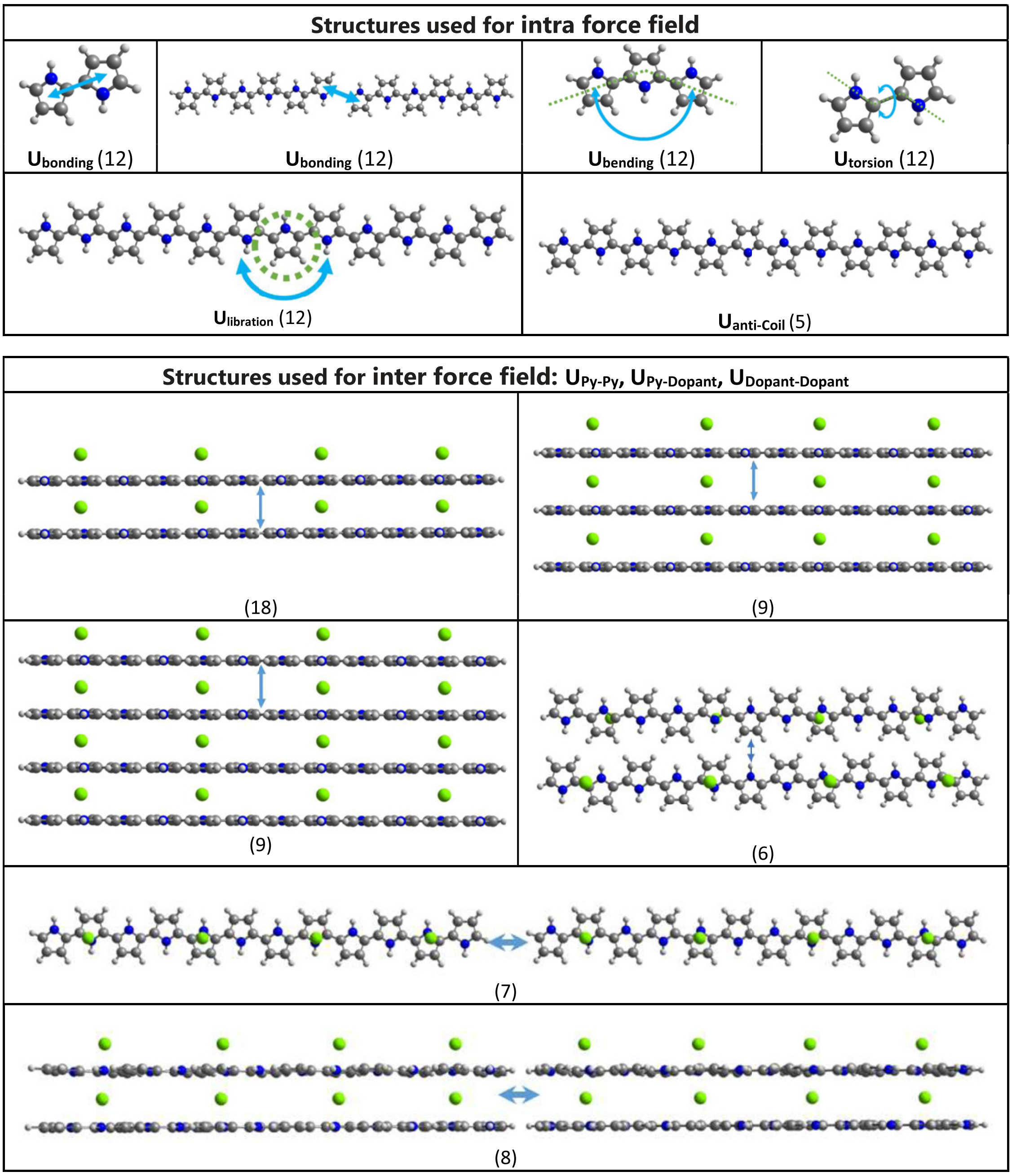

Figure A1. Database of oxidised 12-Py structures analysed with DFT and used in the nonlinear least squares fitting of the FF parameters as described in section 2.

condensed phases. We have adopted a hybrid strategy of relying on a traditional parametrization combined with condensed system simulations for evaluating the various parameters performance. Indeed, the approach has been central for the progressive refinements of the interactions between the polymer and the dopants and for further fine-tuning crucial parameters against condensed phase experimental data.

Along the parameter fitting process we found a need for restoring some balance between the local strong electrostatic attraction areas in the vicinity of dopants and the monomer–monomer interactions between oligomers where electrostatic and dispersion terms need careful combination, shown in figure 4(a). One of the important vindications of the parametrisation approach taken here was that despite their $+4e$ charge, the 12-Py oligomers still attract themselves within a distance of about 7.5 Å, as shown in figure 4(a) but have their minimum around 5 Å consistent with average distances between chains of 4.4 Å measured from x-ray diffraction analysis [17]. This fact enables the system to reach the high densities observed in experiments [16, 21].

In summary, in this work we put forward a new FF for oxidised PPy with anionic chlorine dopants. The parametrisation strategy is described in detail including flowcharts of the concatenated protocol steps. The simulated thermodynamic properties of the condensed phase at ambient temperature are in excellent agreement with experiments, a rare quality of many

FFs. The obtained solid sample displays strong polymer stacking and a preferential ordering of the oligomers along one direction. However, the obtained samples are not crystalline, in agreement with synthesised samples [17]. The FF is generalisable to PPy with other dopants when a re-parametrisation of the inter potential terms is carried over. The FF analytic terms are generalisable to polymer systems that give rise to bipolarons in which regions of consecutive monomers within each oligomer sustain a charge of $+2e$ countered by anionic dopants. The FF is a coarse grained approach, implying a factor of 3–4 savings in computational cost to be weighed against the all-atom FFs expenditures for large systems. We expect to report in the near future on a custom computational implementation that enables simulations of systems two orders of magnitude larger than the one described therein. Currently, the FF introduced here is reliable and certainly useful for the calculation of other properties including the PPy behaviour in composite materials.

Acknowledgments

EBB acknoledges past partial support from the National Science Foundation (USA), grant CHE-0626111. Computations were done in ARGO, the supercomputing cluster of the Office of Research Computing of George Mason University (USA).

Data availability statement

The data that support the findings of this study are available upon reasonable request from the authors.

Appendix A

Figure A1 gives the structures used for calculating the DFT binding energies used in the fitting process of the FF parameters. The arrows in each of the structures indicate the distance or angle that were varied in order to obtain the target points for the fit. Each calculated target point comprises a given geometry and its corresponding DFT binding energy on which the parameters of the model analytical expression are fitted on. For the bending contribution, for example, first the full optimised structure of 12-Py^{+4} was used to equate the r_0 in equation (3) to be the average distance between the contiguous monomers centres of mass. Next, the dimer structures 2-Py^{+1} were used to obtain a first fit of parameters D_e and α in equation (3), which in turn were used as initial values for re-fitting them on 12 target structures of the full 12-Py^{+4} with elongated distance between the 6th and 7th monomers. As a third attempt, the latter parameter values were used as initial points for now fitting on both structures target points together, 24 in total. We note that the electronic energy points calculated for the dimer were referred to the energy obtained at the minimum. For the bending and torsion terms, both the dimer and trimer were cations, 3-Py^{+1} and 2-Py^{+1}. We note that r_0 and γ_0 resulted from the DFT optimisation of 12-Py^{+4} and were not adjustable by the fitting algorithm. The anti-coil term was adjusted on 5 target points from the DFT intermediate geometries reached during the optimisation of the full oligomer. The workflows of figures 5(a) and (b) indicate the successive steps and refitting attempts needed along the process of selecting final values for the 17 adjustable parameters for each fixed value of κ.

ORCID iDs

Estela Blaisten-Barojas https://orcid.org/0000-0003-3259-1573

References

[1] McNeill R, Siudak R, Wardlaw J and Weiss D 1963 *Aust. J. Chem.* **16** 1056–103

[2] McGinness J, Corry P and Proctor P 1974 *Science* **183** 853–5

[3] Unni S M, Dhavale V M, Pillai V K and Kurungot S 2010 *J. Phys. Chem.* C **114** 14654–61

[4] Gracia R and Mecerreyes D 2013 *Polym. Chem.* **4** 2206–14

[5] Wasim F, Kosar N, Mahmood T and Ayub K 2018 *J. Mol. Model.* **24** 1–14

[6] Olson T S, Pylypenko S, Atanassov P, Asazawa K, Yamada K and Tanaka H 2010 *J. Phys. Chem.* C **114** 5049–59

[7] Wu J, Wu S and Sun W 2021 *Electrochem. Commun.* **122** 106879

[8] Liu Z *et al* 2011 *Chem. Commun.* **47** 9912–4

[9] Smela E and Gadegaard N 2001 *J. Phys. Chem.* B **105** 9395–405

[10] Smela E 2003 *Adv. Mater.* **15** 481–94

[11] Otero T F and Valero L 2017 *ChemElectroChem* **4** 3276–82

[12] Zheng W, Whitten P G and Spinks G M 2018 *Multifunct. Mater.* **1** 014002

[13] Otero T F 2021 *RSC Adv.* **11** 21489–506

[14] Thompson B C, Moulton S E, Richardson R T and Wallace G G 2011 *Biomaterials* **32** 3822–31

[15] Huang Z B, Yin G F, Liao X M and Gu J W 2014 *Front. Mater. Sci.* **8** 3945

[16] Fonner J M, Schmidt C E and Ren P 2010 *Polymer* **51** 4985–93

[17] Valtera S, Prokeš J, Kopecká J, Vrňata M, Trchová M, Varga M, Stejskal J and Kopecký D 2017 *RSC Adv.* **7** 51495–505

[18] Dai Y and Blaisten-Barojas E 2008 *J. Chem. Phys.* **129** 164903

[19] Dai Y and Blaisten-Barojas E 2010 *J. Chem. Phys.* **133** 034905

[20] López Cascales J J and Otero T F 2005 *Macromol. Theory Simul.* **14** 40–8

[21] Oliveira Costa S D and López Cascales J J 2010 *J. Electroanal. Chem.* **644** 13–9

[22] Berendsen H J C, van der Spoel D and van Drunen R 1995 *Comput. Phys. Commun.* **91** 43–56

[23] Dong X and Blaisten-Barojas E 2006 *J. Comput. Theor. Nanosci.* **3** 118–27

[24] Bof Bufon C C, Vollmer J, Heinzel T, Espindola P, John H and Heinze J 2005 *J. Phys. Chem.* B **109** 19191–9

[25] Chance R R, Brédas J L and Silbey R 1984 *Phys. Rev.* B **29** 4491–5

[26] Grimme S, Antony J, Ehrlich S and Krieg H 2010 *J. Chem. Phys.* **132** 154104

[27] Raghavachari K, Binkley J S, Seeger R and Pople J A 1980 *J. Chem. Phys.* **72** 650–4

[28] Singh U C and Kollman P A 1984 *J. Comput. Chem.* **5** 129–45

[29] Besler B H, Merz K M and Kollman P A 1990 *J. Comput. Chem.* **11** 431–9

[30] Frisch M J *et al* 2009 *Gaussian 09 Revision E.01* (Gaussian Inc. Wallingford CT, USA)

[31] Levenberg K 1944 *Q. Appl. Math.* **2** 164–8

[32] Marquardt D W 1963 *J. Soc. Ind. Appl. Math.* **11** 431–41

[33] Metropolis N, Rosenbluth A W, Rosenbluth M N, Teller A H and Teller E 1953 *J. Chem. Phys.* **21** 1087–92

[34] Hall C, Ji W and Blaisten-Barojas E 2014 *J. Comput. Phys.* **258** 871–9

[35] Helmick G, Abere Y and Blaisten-Barojas E 2021 The caloric curve of polymers from the adaptive tempering Monte Carlo method *Advances in Parallel & Distributed Processing and Applications* (*CSCE'20 Proceedings*) ed H R Arabnia *et al* (Berlin: Springer) pp 253–60

[36] Frenkel D and Smit B 2002 *Molecular Simulation* (New York: Academic)

[37] Wolf D, Keblinski P, Phillpot S R and Eggebrecht J 1999 *J. Chem. Phys.* **110** 8254–82

[38] Stone A 2013 *The Theory of Intermolecular Forces* (Oxford: Oxford University Press)

[39] Ansari R 2006 *J. Chem.* **3** 186–201

[40] Rudajevová A, Varga M, Prokeš J, Kopecká J and Stejskal J 2015 *Acta Phys. Pol.* A **128** 730–7

[41] Yussuf A, Al-Saleh M, Al-Enezi S and Abraham G 2018 *Int. J. Polym. Sci.* **2018** 1–8

[42] Chemical Retrieval on the Web (CROW) Polymer properties database 2015 www.polymerdatabase.com/polymers/polyethyleneglycol.html

[43] Wohlfarth C 2016 *CRC Handbook of Chemistry and Physics* ed W Hayne (Boca Raton, FL: CRC Press)